# Direct Measurement of the in situ Developed Latent Image: the Residual Swelling Fraction[§]

Vivek M. Prabhu*[,a], Bryan D. Vogt[a], Shuhui Kang[a], Ashwin Rao[a], Eric K. Lin[a],
Sushil K. Satija[b], Karen Turnquest[c]
[a)] Polymers Division, [b)]Center for Neutron Research, National Institute of Standards and Technology,100 Bureau Dr, Gaithersburg, MD 20899
[c)]SEMATECH, 2706 Montopolis Dr, Austin, Texas 78741

**Abstract**

The spatial distribution of polymer photoresist and deuterium labeled developer highlights a fraction of material at a model line edge that swells, but does not dissolve. This residual swelling fraction remains swollen during both the *in situ* development and rinse steps uncovering that the final lithographic feature is resolved by a collapse mechanism during the drying step. We demonstrate that contrast variant neutron reflectivity provides a general method to probe the nanometer resolved *in situ* development and rinse process step.

## I. Introduction

The drive to sub-32 nm critical dimensions places an increasing reliance on chemically amplified photoresists[1]. The process by which a well defined photoacid distribution reacts with photoresist to form a chemical latent image are controlled by a combination of optical and photoresist design parameters. However, a possible trade-off among resolution, exposure dose sensitivity, and line edge roughness (LER) may limit photoresists from reaching sub-2 nm LER[2-7]. A central assumption in these resolution limit models is that the final feature quality is a direct transfer of chemical deprotection statistics due to the combined effects of initial acid distribution and reaction-diffusion process[8,9]. The trends of this statistical approach applied to photoresist resolution limits is supported by computer simulation[10] and lithographic measurements[11].

A critical ionization model for the development step defines the threshold deprotection fraction at which resist polymer dissolves[9,12]. Hinsberg et al. have characterized photoresist polymers dissolve via reactive dissolution kinetics often involving a well-defined steady-state swollen layer[13-15]. An extension of this work would be to study the effect of an imposed compositional gradient such as would appear at a lithographic feature edge. Simulations along these lines uncover relationships between aerial image quality and roughness applying a critical ionization model (threshold development). In this case, the advancing dissolution front faces a transition of soluble to insoluble species. Since the

[§] Official contribution of the National Institute of Standards and Technology; not subject to copyright in the United States
* vprabhu@nist.gov; tele (301) 975-3657; fax. (301) 975-3928

Advances in Resist Materials and Processing Technology XXIV, edited by Qinghuang Lin
Proc. of SPIE Vol. 6519, 651910, (2007) · 0277-786X/07/$18 · doi: 10.1117/12.712311

surface swollen layer transient appears during bulk development a question remains as to what happens as the bulk development ceases[16,17] near the so-called solubility switch. Further, this transition zone will result from the initial deprotection latent image which can be controlled by aerial image, polymer chemistry, photoacid generator and base additives, and post-exposure bake conditions[18-21].

Recent measurements of the latent image[20,21] have independently validated several physically based models[22-24] for the reaction diffusion process. However, the mechanism by which the latent images dissolves revealing a final structure could only be correlated or inferred by scanned probe microscopy in model materials, or scanning electron microscopy in lithography studies. Visible light reflectance is capable of quantifying both the kinetics and spatial distribution of swelling on the ms time scale and quarter wavelength length scale. However, as the layer become both thin and rough this approach loses sensitivity. This problem can be circumvented by using radiation of smaller wavelength such as with neutrons or x-rays. In order to perform *in situ* measurements of photoresist films in contact with liquids, neutrons are preferred due to negligible absorption and scattering by the liquid phase.

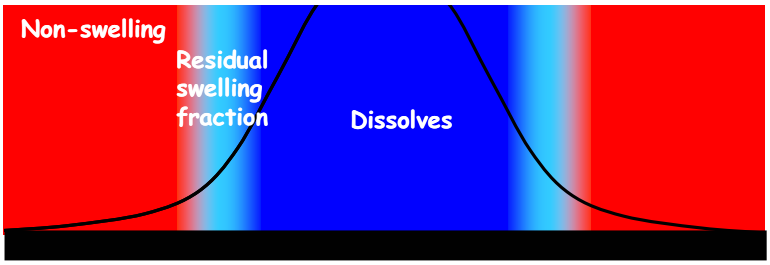


Scheme 1. Schematic of the deprotection profile (solid line) that appears as a gradient line edge with "solubility switch" for development and residual swelling fraction appearing between non-swelling and dissolving photoresist regions.

In this paper, we provide the first direct measurement of the residual swelling fraction (RSF) at a model lithographic line edge as shown in Schematic 1. This fraction of material is defined by the solubility switch and a lower composition limit for swelling without dissolution. It is demonstrated that the line-edge region remains diffuse over length scales exceeding the single chain dimensions upon completion of hydroxide development and water rinse step. The RSF spatial extent subsequently collapses upon drying. This new evidence supports a dynamic interface, but with physical grounds extendible to modern simulations[8,25,26] and perhaps can lead to rationalized approaches to minimize the residual swelling fraction by resist design and additives-based approaches to smooth and reduce LER.

## II. Experimental

A well-defined latent image was prepared by successive spin coating of a photoresist/acid feeder layer bilayer structure. This provides a sharp initial photoacid step profile and subsequent acid catalyzed deprotection of the underlying photoresist polymer. This reaction front was characterized with nanometer resolution[20] by neutron reflectivity. Here, we use these model line-edge systems for the *in situ* development, rinse, and subsequently dried samples; this enables direct measurements of the line edge structure in contact with developer. Alternatively, the surface exposure in a resist

thin film with a highly absorbing wavelength is a more general method that avoids complications of finding suitable casting solvents for the bilayer structure[22,27].

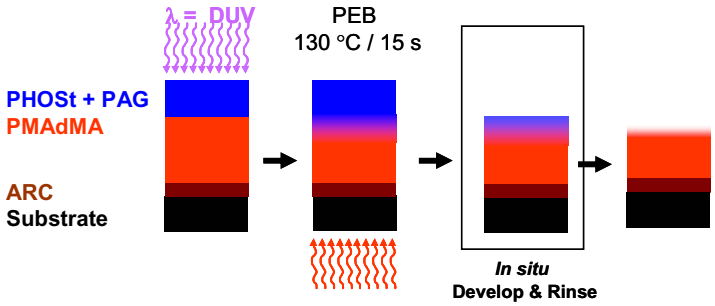


Scheme 2. Sample processing from UV exposure, post-exposure bake, in situ development and rinse steps, and final dried state.

**Materials and Sample Preparation**

The acid feeder layer / photoresist polymer bilayer films were prepared with one slight modification; an antireflective coating (ARC) was applied to improve the adhesion of the photoresist polymer to the clean silicon substrate for the in situ development studies. Therefore the sample is a trilayer subject to in situ development as shown in Scheme 2. The ARC was a diluted form of CD2326 (Brewer Science Inc.) spun coat onto the cleaned silicon wafer with regrown native oxide and post-apply baked (PAB) at 200 °C for 5 min under a $N_2$ blanket. The model photoresist polymer poly(methyladamantyl methacrylate) (PMAdMA) with number-average molecular mass ($M_n$) of 8800 g mol$^{-1}$ and polydispersity index of 1.18 (DuPont Electronic Polymers) was spin cast from toluene onto this ARC layer followed by a PAB of 130°C / 60 s. The acid-feeder layer consists of poly(4-hydroxystyrene) (PHOSt) (DuPont Electronic Materials, $M_n$ = 8000 g mol$^{-1}$) with 5 % by mass of triphenylsulfonium perfluorobutanesulfonate spun coat from 1-butanol and PAB at 130 °C / 60 s. This trilayer is then exposed to broadband ultraviolet (UV) radiation (300 mJ/cm$^2$) and post exposure baked at 130 °C for 15 s. The deprotection reaction scheme for the PMAdMA is provided in Figure 1. The deprotection reaction extent into methacrylic acid (MAA) and residual methylene adamantane was characterized by infrared spectroscopy [20,28]. Control samples without UV exposure and post exposure bake were prepared to characterize the initial sharp trilayer structure. Excellent reproducibility of film thickness between different samples processed under the same conditions were achieved and observed by characterization by infrared spectroscopy and neutron reflectivity.

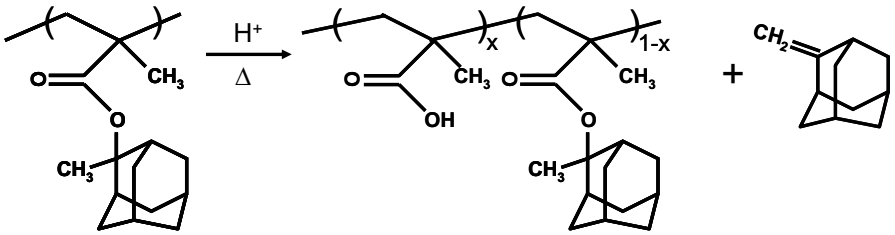


Figure 1. Acid catalyzed deprotection reaction for the model 193 nm photoresist polymer Poly(methyladamantyl methacrylate) into poly(methacrylic acid – co – methyladamantyl methacrylate) and methylene adamantane residual product.

**Specular Neutron Reflectivity**

Neutron reflectivity measurements were performed on the NG-7 reflectometer at the National Institute of Standards and Technology Center for Neutron Research. The absolute reflected neutron intensity was measured as a function of the scattering wave vector ($Q$) normal to the film, $Q = 4\pi\lambda^{-1} \sin\theta$, where $\lambda$ is the fixed incident neutron wavelength of 4.75 Å and $\theta$ is the angle of reflection. The specular reflected intensity provides nanometer resolution depth profile of the film due to neutron scattering length density variations between components.

***In situ* Latent Image**

The trilayer sample was characterized by neutron reflectivity on unexposed and post-exposure baked samples. As the deprotection reaction proceeds the difference in hydrogen content between PHOSt and PMAdMA and subsequent deprotection reaction provides sufficient neutron contrast to measure the reaction front[20] and film profile. Deuterium labeling, however, provides substantial contrast enhancement due to the difference in scattering lengths of the H ($-0.37 \times 10^{-12}$ cm) and D ($0.67 \times 10^{-12}$ cm) nuclei. The physical thickness (mass density) and surface roughness of the films is measured using x-ray reflectivity.

***In situ* development and rinse**

*In situ* development was performed on the well-defined latent image reaction fronts. These samples were placed into a custom liquid cell and a single sample was subject to in situ development and rinse. Two trilayer separate samples were measured to characterize the polymer segmental profile and the deuterium labeled tetramethylammonium profile using a full contrast and zero-average contrast approach, respectively[16].

Full contrast experiments used protonated 0.065 *N* tetramethylammonium hydroxide (TMAH) prepared from the salt form (Aldrich) in $D_2O$ (99.9 % isotopic purity, Aldrich) to maximize the scattering length contrast between polymer and solvent. Once developer was introduced into the cell the acid feeder layer and portion of the reaction front dissolved as observed visually through a view port in the liquid cell. The developed structure remaining in contact with the developer was measured by specular neutron reflectivity. Subsequently the developer was removed out of the cell was rinsed and filled with $D_2O$ to mimic the rinse step and the second measurement completed in contact with $D_2O$.

For the zero-average contrast experiment, a $D_2O$ / $H_2O$ mixture of 0.197 volume fraction $D_2O$, which contrast matches the dry polymer film ($Q_C^2$ of $4.0 \times 10^{-5}$ Å$^{-2}$), containing 0.065 *N* deuterium labeled $d_{12}$-tetramethylammonium (*d*-TMA) hydroxide prepared from the salt form (Cambridge Isotopes, Andover MA) was equilibrated with the film. Analogous to the full contrast experiment, the sample was measured after development, but then subject to two types of in situ rinses the first with the zero-average contrast solvent to detect any trapped *d*-TMA and then with $D_2O$. After the development experiments were completed the films removed from the liquid cell, tilted to allow the water to drain easily and dried in open air. The change in film thickness from the original trilayer was observed visually and subsequently measured by neutron and x-ray reflectivity.

These experimental data are fit to reflectivity profiles calculated from model scattering length density profiles ($Q_c^2 = 16\pi \sum b_i / v$) using the Parratt algorithm,[29] where the scattering length of each repeat unit is determined by the sum over the atomic scattering lengths $b_i$ within molar volume ($v$) leading to the absolute scattering length density, an intensive absolute quantity. In general, this approach uses successive layers (a box model) of constant $Q_C^2$ with interface smeared by a Gaussian function leading to error function interfacial width profiles. For dry films each component (silicon, silicon oxide, ARC, and polymer) is quantitatively determined using layers of constant absorption coefficient, scattering length density, and thickness. However, for liquid and base immersed films, the polymer and base profiles are inadequately represented by one layer, so two to three layers are needed to describe the non-uniformities at the solid / liquid interface. The calculated reflectivity from the trial $Q_C^2$ profile is fit to the experimental data using a Levenberg-Marquardt non-linear least squares method with adjustable thickness, scattering length densities, and interfacial width of the unknown layers with least-squares statistic ($\chi^2$). These $Q_C^2$ profiles can be directly converted to volume fraction profiles. Uncertainties are calculated as the estimated standard deviation from the mean. In the case where the limits are smaller than the plotted symbols, the limits are removed for clarity.

## III. Results and Discussions

The photoacid catalyzed deprotection reaction front broadens an initially sharp interface (model line edge) due to photoacid diffusion. The neutron reflectivity results for unexposed and post-exposure baked samples are similar to that examined elsewhere and only the final results are reported. The dry film thickness corresponds to 26 nm of ARC, 124 nm of PMAdMA and 61 nm of acid feeder layer. The deprotection profiles in terms of fraction of MAA are obtained by combining neutron reflectivity with *infra*red spectroscopy[20]. Figure 2 highlights the main results of the photoresist latent image comprised of an initial sharp MAdMA profile (solid line) and MAA deprotection fraction (dotted line) formed by the acid catalyzed reaction of Figure 1. The photoacid diffuses from the acid feeder layer (not shown for clarity) deprotecting PMAdMA leading to the broad latent image profile. The resulting deprotection profile is smooth and continuous because this measurement averages in the plane of the film. Hence any heterogeneity in deprotection that occurs along the interface (in-plane) is averaged by the specular reflectivity technique.

The in situ develop, rinse, and dried samples are shown in the composite plots of Figure 3. The developed latent image remaining in contact with 0.065 *N* TMAH in $D_2O$ was measured by a full contrast study as shown at the topmost dataset. The reflectivity arises from the interferences from the developer/resist, resist/ARC and ARC/silicon substrate interfaces. The four prominent fringes that appear after the critical edge correspond to the thinnest ARC layer which gives rise to the longest wavelength fringes due to the inverse relationship between film thickness ($D$) and fringe period ($D = 2\pi/\Delta Q$). However, as can clearly be seen there are additional fringes of higher frequency convoluted near the maxima of the long-wavelength fringes. These correspond to the total film structure which is resolved by fitting the data to a multilayer stack resulting in the scattering length density profile to the immediate right in Figure 3b. The

ordinate is the absolute scattering length density plotted versus distance whereby the abscissa has been shifted to place the ARC/resist interface at zero. The silicon substrate appears with $Q_c^2$ of 1.06× $10^{-4}$ Å$^{-2}$ transitioning through the silicon oxide, ARC, resist polymer, and finally the developer ($Q_c^2$ = 3.16 × $10^{-4}$ Å$^{-2}$).

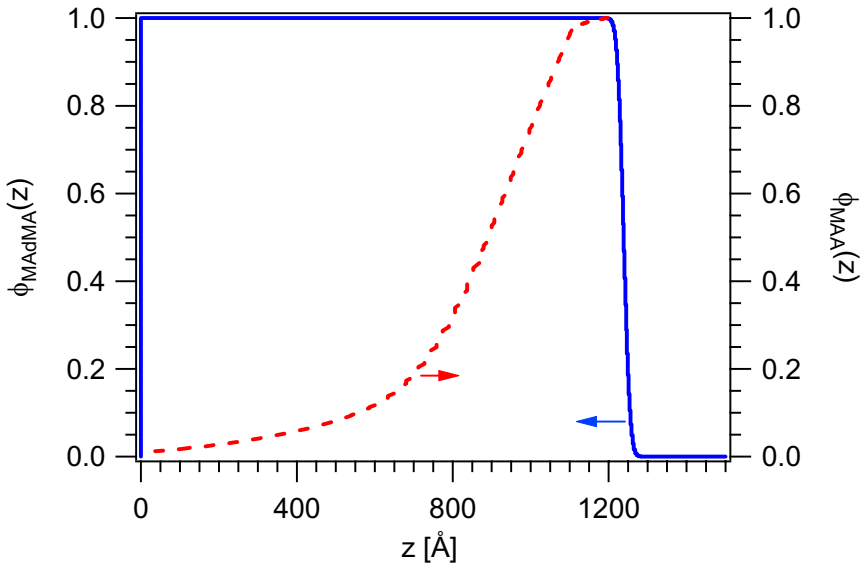


Figure 2. Neutron reflectivity results analyzed in terms of volume fraction profiles for initial sharp MAdMA profile (solid line, left axis) and partially deprotected (MAA) (dotted line, right axis) profiles after a post exposure bake at 130°C of 15 s. The photoacid reaction diffusion from the acid feeder layer partially deprotects PMAdMA as shown by the smooth MAA profile as a function of distance *z* from the underlying antireflective coating.

The thin ARC layer fringes of thickness 28 nm are persistent due to the large $Q_C^2$ difference and sharp interfaces with the silicon substrate and resist polymer. The ARC/resist interface remains sharp with interfacial width of 12 Å indicating negligible intermixing as expected between cross-linked network/polymer interfaces. However a very diffuse resist/developer interface is required to fit the data. This provides a first indication that the initial broad latent image remains highly diffuse even upon development. The resist/developer interface is diffuse because the lack of persistence of fringes associated with the thicker polymer layer. The non-swelling portion of the resist polymer has a scattering length density equal to the dry state indicating no appreciable water sorption in this phase.

Continuing with this sample the in situ rinse with $D_2O$ is shown as the third reflectivity curve from the top in Figure 3a. In this case the features look very similar to the in situ developed films; however, slight differences appear in the prominence of the interference fringes between (0.025 and 0.035) Å$^{-1}$ and mid-$Q$ region. The $Q_C^2$ profiles have an identical substrate and ARC profile, when compared to the developed case. However, the modification of the resist/developer interface accounts for the subtle reflectivity differences in terms of a reduced swelling interfacial width by 2 nm, but maintaining a diffuse interface.

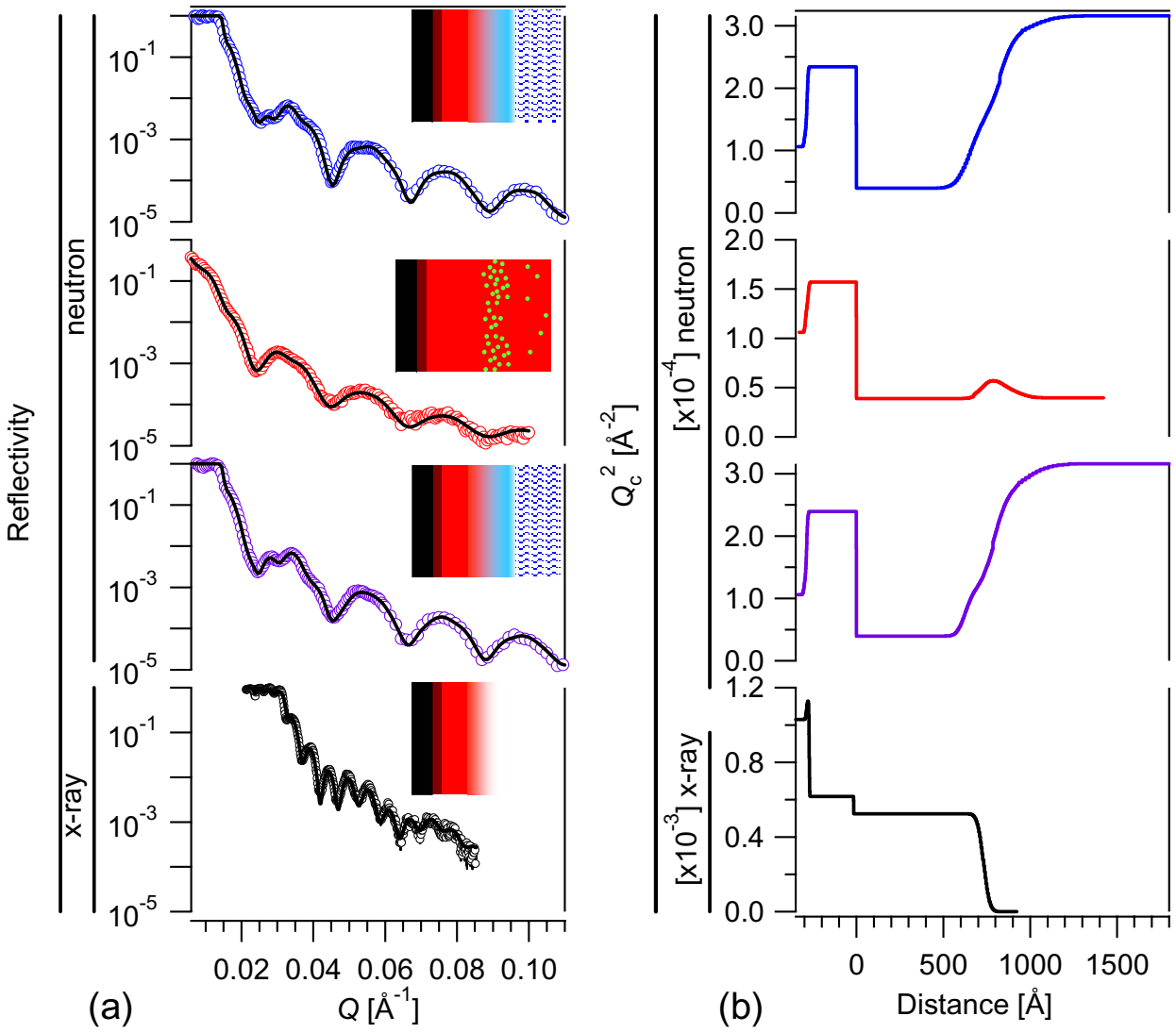


Figure 3. (a) Neutron and x-ray reflectivity measurements with model fits in order from top to bottom highlighting the swollen polymer film and deuterium labeled tetramethylammonium counterion profile under 0.065 N TMAH in situ conditions, swollen polymer film under water rinse conditions and finally *ex situ* dried thin film. The corresponding scattering length density profile of the multilayer thin film structure shown in (b) includes the silicon substrate, native silicon oxide, antireflective coating (ARC) and overlying polymer thin film in contact with aqueous solutions for in situ development conditions. All distances are relative to the ARC / polymer interface.

The weakly acidic MAA groups must sustain interfacial swelling in $D_2O$, therefore the predominant resist residual swelling fraction collapse does not occur during this rinse step. In fact, the final dry feature measured by x-ray reflectivity is shown at the bottom of Figure 3a. The dried feature shows reflectivity fringes associated with the total film thickness. The persistence of the fringes indicates relatively low physical roughness, when compared to the in situ conditions. The scattering length density profile for x-rays is shown in Figure 3b. In this case the silicon substrate appears with $Q_c^2$ of $1.02\times 10^{-3}$ Å$^{-2}$ transitions through the silicon oxide, ARC, polymer, and finally air ($Q_c^2 = 0$). The physical density profile of the polymer layer is significantly thinner than the in situ compositional profiles from neutron

reflectivity. Therefore the highly extended residual swelling fraction undergoes a collapse mechanism to the final feature critical dimension and roughness during drying.

The previous experiments highlighted the total film behavior by using deuterium oxide as the solvent which provides a large scattering length density difference with the film components. However, if the scattering length density of the solvent is reduced to the polymer photoresist, via isotopic mixtures, the film is contrast matched. Therefore the resist film is invisible to neutrons due to the lack of contrast[30] with the solution. Upon addition of deuterium-labeled developer to this contrast matched solution its local distribution may enhance reflectivity because the d-TMA molecule has a high $Q_c^2$.

The reflectivity for this contrast match condition for development with 0.065 *N* d-TMAH is shown in Figure 3a second dataset from the top. In this case the lack of a critical edge is due to $Q_c^2$ of the solvent lower than silicon. However, reflectivity is still observed due to the presence of the ARC layer that provides contrast with the substrate and polymer film. The ARC layer was within 0.5 nm in thickness with the full contrast study experiment. The first reflectivity maxima are distorted appearing as a doublet. In order to accommodate the additional fringe detail, the contrast must appear in the vicinity of the developer/resist interface as shown in Figure 3b. The solvent and non-swelling resist zone has the same $Q_c^2$, but an interface with an extrema is required to resolve the features of the reflectivity data. The interfacial enhancement is provided by the high scattering length deuterium labeled tetramethylammonium developer cations. Therefore at the developer step within the residual swelling fraction, an excess of *d*-TMA ions appears at the diffuse interface. This is consistent with the acid-base titration of the weakly acidic MAA groups due to the strong coupling between polyion and counterion observed in model cases of polyelectrolytes in thin films[16] as well as in semidilute solutions[31]. These measurements complement the real-time infrared spectroscopy study within the steady state gel layer[13], but within the final developer residual swelling fraction.

***Component Concentration profiles***

The segmental volume fraction profiles are obtained by combining the full contrast and zero average contrast experiments. The $Q_C^2$ profile as shown in Figure 3b for the polymer and deuterium labeled TMAH experiments can be expanded into contributions from the polymer ($\phi_p$), solvent ($\phi_s$), and base ($\phi_B$) such that,

$Q_{c,FC}^2(z) = \phi_p Q_{c,p}^2 + \phi_s Q_{c,s}^2 + \phi_B Q_{c,h-TMA}^2$ and $Q_{c,ZAC}^2(z) = \phi_p Q_{c,p}^2 + \phi_s Q_{c,s}^2 + \phi_B Q_{c,d-TMA}^2$ for the full contrast and zero-average contrast experiments, respectively. The only difference is the $Q_C^2$ of the deuterium labeled base *d*-TMA ($4.2 \times 10^{-4}$ Å$^{-2}$) contrasts the protonated TMA ($-3.2 \times 10^{-5}$ Å$^{-2}$). The physics of the problem should lead to equivalent volume fraction profiles between the two sets of experiments. Using an incompressible assumption for the mixing of the species ($\phi_p + \phi_s + \phi_B = 1$) the base and polymer profiles are determined by

$$\phi_B(z)=\frac{Q^2_{c,ZAC}(z)-Q^2_{c,p}}{Q^2_{c,d-TMA}-Q^2_{c,p}} \quad \text{and} \quad \phi_p(z)=\frac{Q^2_{c,FC}(z)-Q^2_{c,s}-\phi_B(Q^2_{c,h-TMA}-Q^2_{c,s})}{Q^2_{c,p}-Q^2_{c,s}}$$ . The base profile is obtained directly because $Q_C{}^2{}_p$ and $Q_C{}^2{}_s$ are equal, while the volume fraction profile of the base is required to analyze the polymer profile. The raw experimental data in Figure 3b provides all the physical length scales. However, the conversion to the volume fraction profiles highlights the concentration regimes that occur at the line edge due to residual swelling fraction as illustrated in Figure 4a.

The volume fraction profiles ($\phi_i$) for each component are plotted as $\phi_i$ versus distance from the ARC / resist interface. The polymer segment profile resolves the dense non-swollen region and transition to the RSF. The concentrated dense phase ($\phi \approx 1$) to semidilute and dilute regimes are observed. A long tail in polymer concentration even occurs in a dilute solution regime assuming a homogeneous phase. This implies that the low molecular weight polymers must associate to form the swollen line edge. This is reminiscent of associating polymers whereby a large chemical mismatch (such as hydrophobicity) can drive and maintain association, rather than dispersion. In such a case the entropy gained by dissolving into the solution cannot overcome the association energy due to the hydrophobicity. This general scheme to determine the nature of a swollen line edge can be applied to a variety of classes of materials to test the extent of hydrophobic content, copolymer chemistry, and molecular weight on residual swelling fraction. These experiments may also be applied to test the concept such as pixel size between polymeric and molecular glass resist, since the concept of a pixel applies during the development step.

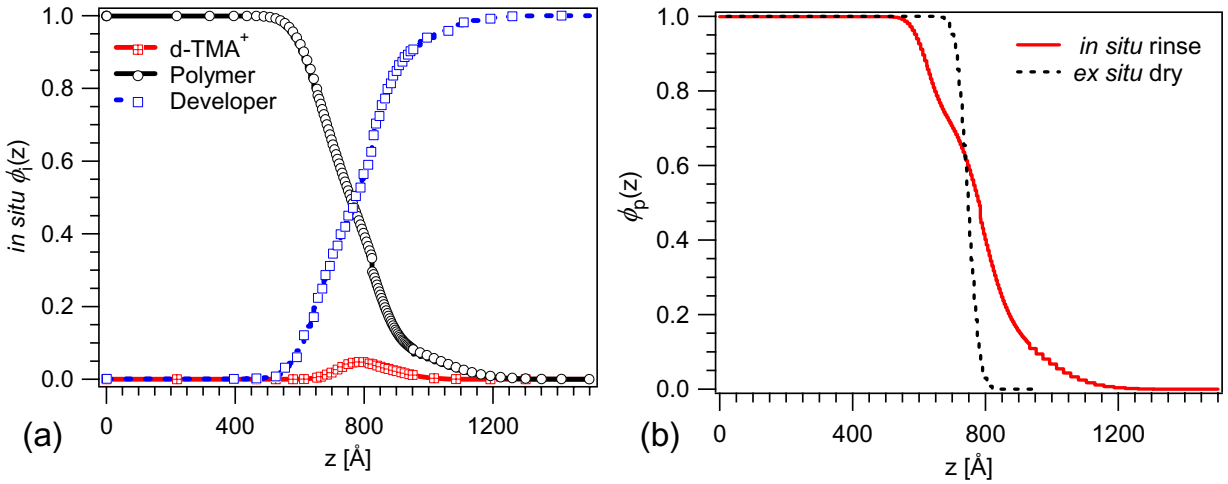


Figure 4. (a) Characterization of the *in situ* development volume fraction profiles for the polymer segment, $D_2O$, and deuterium labeled tetramethylammonium counterion (d-TMA$^+$) as a function of distance from the antireflective coating / polymer interface. (b) *In situ* rinse and *ex situ* dry polymer composition profiles measured by neutron and x-ray reflectivity, respectively. The swollen line-edge collapses with feature roughness of 7 nm determined by x-ray reflectivity.

The lower composition limit for swelling from the polymer segment profile (Figure 4a) appears at a depth of 54 nm corresponding to a MAA fraction of 0.095 from the dry latent image (Figure 2). Therefore the deprotection limit for the

residual swelling fraction is lower than that determined from single layer films[32]. In the single layer case the initial photoacid distribution is uniform and the deprotection process leads to chemically heterogeneous films which at low deprotection extents are comprised of well-separated deprotection domains. These diffuse deprotection domains percolate and overlap[33] with post-exposure bake reaction time. The percolation of MAA domains was correlated with the onset of swelling at an average deprotection extent near 30 %. However at the feature line-edge the photoacid diffusion from the acid feeder layer will lead to a highly connected or percolated structure as the photoacid follows multiple diffusion paths defined by the protected and deprotected species[22]. The resulting broad interface completely dissolves at the solubility switch, but water and developer will swell to the lower composition limit (0.095 fraction MAA). The data appear to provide an insight that below this deprotection level water and developer are effectively excluded. This may arise from two possibilities. The MAA groups are randomly distributed; hence the films are too hydrophobic to allow unfavorable water-MAdMA contacts. Alternatively, the hydrophilic MAA are non-uniformly distributed into isolated pockets[26] or channels[34,35] such that while water can find a pocket of hydrophilic moieties, the surrounding hydrophobic matrix prevents volume expansion.

The *d*−TMA profiles achieve a peak concentration of 5 % by volume. The *d*−TMA concentration is enriched over the bulk volume fraction (0.55 % by volume) because of the high concentration of weakly acidic MAA groups within the residual swelling fraction. The process by which *d*−TMA is enhanced is partially due to the local titration of the high concentration of MAA segments that appear in the dry latent image. The decay of the *d*−TMA profile to zero perhaps comes as a slight surprise considering the finite deprotection extent towards the substrate (Figure 2) expected by the latent image. The further suppression of TMA in addition to water within the RSF is likely due to the additional requirement for the TMA ion to carry its hydration shell[36,37]. The effect of image charge is also a possible due to the dielectric constant difference between the pure MAdMA polymer and the water ions. The free and mobile ions observe an effective repulsive potential set up by the dielectric constant difference. This effect has been speculated at the polymer / silicon substrate, but holds a much wider range in physical phenomenon from the origins of interfacial tension in electrolyte solutions[38] to crucial effects in polyelectrolyte adsorption[39]. The decay of *d*−TMA to the bulk is expected by the low concentration of polymer segments as well as dilute bulk solution concentration.

The *in situ* water rinse, summarized by the experimental data of Figure 4b, illustrates the persistence of swelling. However, there is a slight shrinkage as shown in Figure 4b but the RSF remains highly diffuse. This behavior was not previously known and perhaps modifies the manner in which the development process is viewed. Materials which exhibit true etch-like development fall into a separate class as noted by Hinsberg et al[13]. In the present case the MAA, a hydrophilic moiety, ionizes in water as demonstrated in model polyelectrolyte systems such as brushes and gels. In the present case both the developer and water rinse may be regarded as good solvents for the RSF. In a previous resist generations such as those incorporating hydroxystyrene, the water should be a poor solvent, since PHOSt is not a water soluble polymer. Therefore the swelling collapse should occur more prominently during the water rinse step.

Lastly, the RSF collapse occurs during the drying process (Figure 4b) whereby the physical mass density profile is shown determined by x-ray reflectivity (Figure 3b). In this experiment the thin films were permitted to air dry. This process leads to a substantial collapse of the highly swollen phase. The area under the segmental profiles is the total volume of polymer. Therefore, the final thickness obtained from an ideal collapse can be calculated from a line that partitions equal area. The calculated final thickness with ideal collapse and no interfacial roughness should be 78 nm. However, the experimental data show the film thickness of 75 nm with a surface roughness of 7 nm.

These measurements support a mechanism by which resist polymer chains can rearrange in a dilute swollen phase as well as surface segregate. Therefore the non-ideal collapse can cause segregation of polymer groups based on chemical mismatch (hydrophobicity) or quite possibly through the mechanism of film drying.

## IV. Conclusions

Insight into the mechanism of development, rinse, and drying at a gradient line edge was measured by neutron reflectivity with nm resolution. The direct measurements highlight a residual swelling fraction during the development and rinse process steps with a lower composition limit for swelling at a gradient interface which differs from single layer films. Evidence directs to a highly associated and swollen polymer resist phase present at the line-edge region during development. The swelling persists during the water rinse step and collapse of the diffuse residual swelling fraction during the drying process leads to the final surface roughness. A mechanism of a simple transfer of roughness from the latent image to the developed image is challenged by these data due to the swelling and associating polymer layer. Extending these concepts to previous latent image analysis imply the minimization of the residual fraction provides the lowest surface roughness. This can be achieved through resist and optical design to provide the highest latent image profile slope. However, an ideal collapse and complete elimination of surface roughness was not observed in line with lithographic studies. An improved simulation model to capture the nanometer scale effects should include both percolation and penetration of developer and associative behavior due to the heterogeneity and large chemical mismatch of resist components. Future directions of comparing materials of varying hydrophobicity (chemical mismatch) may shed light on minimizing the residual swelling fraction.

## V. Acknowledgments

This work was supported by SEMATECH under Agreement #309841 OF. The authors acknowledge Drs. Jim Sounik and Michael Sheehan at DuPont Electronic Polymers for providing the polymers used in this study.
Certain commercial equipment and materials are identified in this paper in order to specify adequately the experimental procedure. In no case does such identification imply recommendations by the National Institute of Standards and Technology nor does it imply that the material or equipment identified is necessarily the best available for this purpose.

Reference List


(1) Ito, H. *Advances in Polymer Science* **2005,** *172*, 37-245.
(2) Chandhok, M. et al. *Journal of Vacuum Science & Technology B* **2004,** *22* (6), 2966-2969.
(3) Hinsberg, W. et al. *Journal of Vacuum Science & Technology B* **1998,** *16* (6), 3689-3694.
(4) Pawloski, A. R. et al. *Journal of Microlithography Microfabrication and Microsystems* **2006,** *5* (2).
(5) Pawloski, A. et al. *Proceedings of the SPIE, Advances in Resist Technology and Processing XXI* **2004,** *5376*, 414.
(6) Hoffnagle, J. A. et al. *Optics Letters* **2002,** *27* (20), 1776-1778.
(7) Hoffnagle, J. A. et al. *Journal of Photopolymer Science and Technology* **2003,** *16* (3), 373-379.
(8) Schmid, G. M. et al. *Journal of the Electrochemical Society* **2004,** *151* (2), G155-G161.
(9) Tsiartas, P. C. et al. *Macromol.* **1997,** *30*, 4656-4664.
(10) Gallatin, G. M. et al. *Journal of Vacuum Science & Technology B* **2003,** *21* (6), 3172-3176.
(11) Van Steenwinckel, D. et al. *Journal of Vacuum Science & Technology B* **2006,** *24* (1), 316-320.
(12) Houle, F. A. et al. *Macromol.* **2002,** *35* (22), 8591-8600.
(13) Hinsberg, W. et al. *Macromol.* **2005,** *38* (5), 1882-1898.
(14) Hinsberg, W. D. et al. *Proceedings of the 13th International Conference on Photopolymers, Advances in Imaging Materials and Processes, RETEC 2003* **2003,** 193-209.
(15) Hinsberg, W. D. et al. *Proceedings of the SPIE, Advances in Resist Technology and Processing XXI* **2004,** *5376*, 352-359.
(16) Prabhu, V. M. et al. *Langmuir* **2005,** *21* (15), 6647-6651.
(17) Schmid GM et al. *Journal of Vacuum Science and Technology B* **2002,** *20* (6), 2913-2919.
(18) Stewart, M. D. et al. *Proceedings of SPIE* **2000,** *3999*, 665-674.
(19) Stewart, M. D. et al. *Journal of Vacuum Science & Technology B* **2002,** *20* (6), 2946-2952.
(20) Vogt, B. D. et al. *Macromol.* **2006,** *39* (24), 8311-8317.
(21) Vogt, B. D. et al. *Journal of Vacuum Science & Technology B* **2006,** *25*, 175-182.
(22) Houle, F. A. et al. *Journal of Vacuum Science & Technology B* **2000,** *18* (4), 1874-1885.
(23) Houle, F. A. et al. *Journal of Vacuum Science & Technology B* **2002,** *20* (3), 924-931.
(24) Houle, F. A. et al. *Journal of Vacuum Science & Technology B* **2004,** *22* (2), 747-757.
(25) Sarris, V. et al. *Japanese Journal of Applied Physics Part 1-Regular Papers Brief Communications & Review Papers* **2005,** *44* (10), 7400-7403.
(26) Meiring, J. et al. *Proceedings of SPIE* **2005,** *5753*, 350-360.
(27) Hinsberg, W. D. et al. *Proceedings of the SPIE, Advances in Resist Technology and Processing XVII* **2000,** *3999*, 148.
(28) Kang, S. et al. *Polymer* **2006,** *47* (18), 6293-6302.
(29) Parratt, L. G. *Physical Review* **1954,** *95* (2), 359-369.
(30) Wignall, G. D. et al. *Reports on Progress in Physics* **2005,** *68* (8), 1761-1810.
(31) Prabhu, V. M. et al. *Journal of Chemical Physics* **2004,** *121* (9), 4424-4429.
(32) Rao, A. et al. *Langmuir* **2006,** *22* (24), 10009-10015.
(33) Kang, S. et al. *Macromol.* **2007,** *40*, 1497-1503.
(34) Dammel, R. *Diazonaphthoquinone-based resists;* Tutorial Text in Optical Engineering ed.; SPIE - The International Society for Optical Engineering: 1993; Vol. TT 11,
(35) Huang, J. P. et al. *Macromol.* **1989,** *22* (10), 4106-4112.
(36) Garcia-Tarres, L. et al. *Journal of Physical Chemistry B* **1998,** *102* (38), 7448-7454.
(37) Turner, J. et al. *Molecular Physics* **1990,** *70* (4), 679-700.
(38) Onsager, L. et al. *Journal of Chemical Physics* **1934,** *2*, 528-536.
(39) Messina, R. *Physical Review e* **2004,** *70* (5).